# Supplementary Information

10-HDA from royal jelly ameliorates autism-like behaviors by promoting Treg commitment through microbiota-IL-6-driven bivalent histone remodeling

Contents: Supplementary Figures S1-S6 and legends.

Supplementary Figure S1. Supplementary behavioral analyses of RJ-mediated efficacy and HPLC characterization of RJ constituents. (a) Representative HPLC chromatogram of the fatty acid constituents in RJ preparations (RJ1 and RJ2). (b) Schematic illustration of the three-chamber social novelty test, in which the subject mouse could freely explore a chamber containing the previously encountered Mouse 1 or a novel stranger (Mouse 2). (c) Representative movement trajectory plots from the social novelty test, where M1 denotes the chamber with Mouse 1, M2 denotes the chamber with Mouse 2. (d) Quantification of interaction time with Mouse 1 versus Mouse 2 during the social novelty phase in response to RJ1/2 treatment (n = 6). (e) Social novelty test in BTBR mice treated with varying doses of RJ (C57, BTBR, 300, 3000, or 30000 mg/kg; n = 6). (f-h) Quantification of interaction time in the sociability phase (f), social novelty phase (g), and number of marbles buried in the marble burying test (h) in BTBR mice treated with extended RJ doses (3000, 6000, or 9000 mg/kg) (n = 6). (i) Social novelty test in BTBR mice treated with royal jelly protein extract (RJP) or fatty acid extract (RJFA) (n = 6). (j) Social novelty test in BTBR mice treated with 10-HDA or 10-HDAA (n = 6). All data are presented as mean ± SEM. Statistical significance was assessed by two-way ANOVA for three-chamber trials and one-way ANOVA with post hoc multiple comparisons for the marble burying test. $p < 0.05$, $p < 0.01$, $p < 0.001$. ns, not significant.

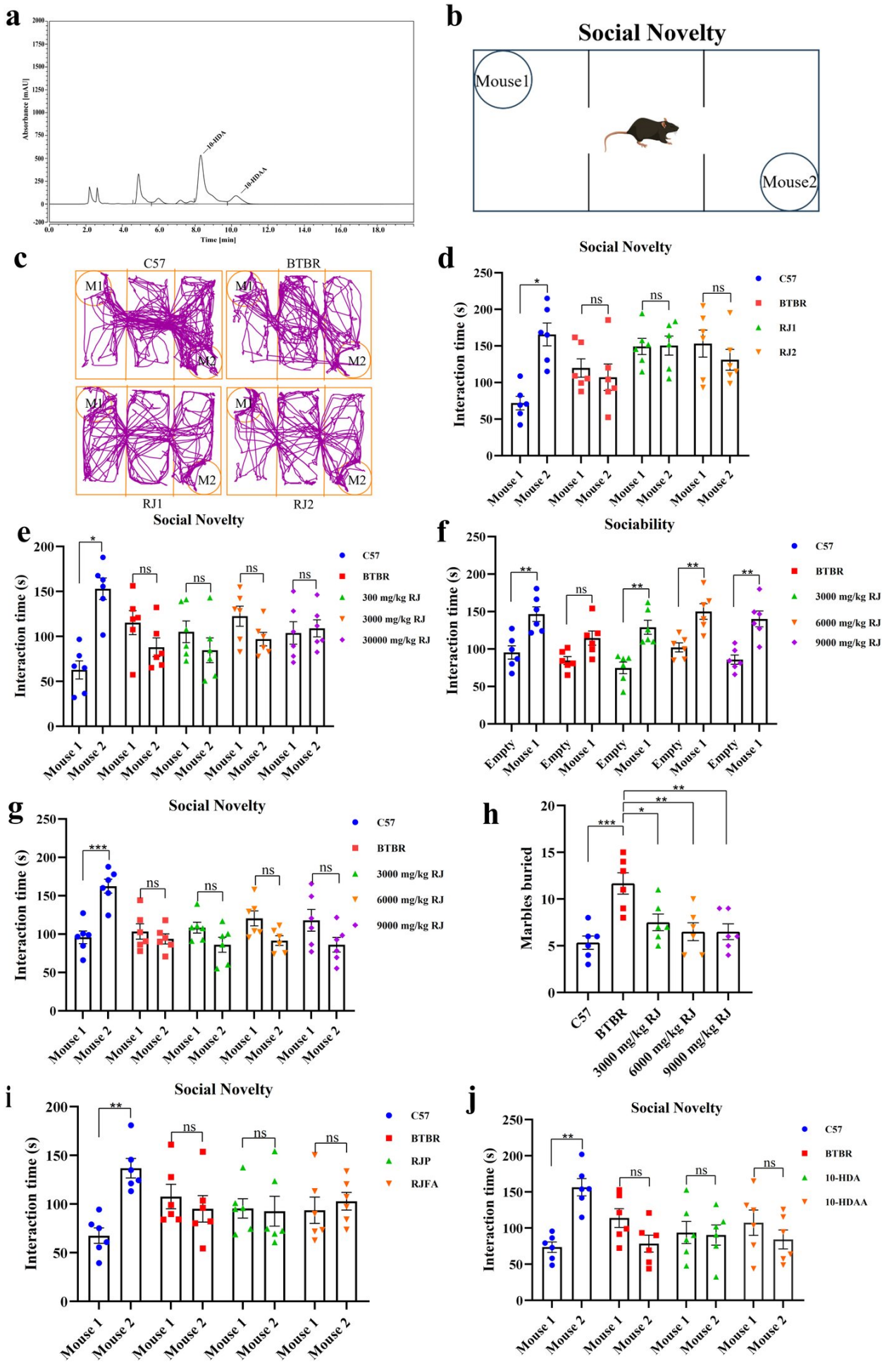


*Supplementary Figure S1*

Supplementary Figure S2. Tissue-dependent Th17/Treg imbalance in BTBR mice. (a-c) Normalized percentage of CD4+Foxp3+ Tregs (b) and CD4+IL-17A+ Th17 cells (c) in the meninges in 10-HDA-treated mice as quantified by flow cytometry (n = 6). Representative flow cytometry plots illustrating the percentage of CD4+Foxp3+ Tregs (upper panels) and CD4+IL-17A+ Th17 cells (lower panels) in the meninges were shown in (a). (d-f) Normalized percentage of CD4+Foxp3+ Tregs (e) and CD4+IL-17A+ Th17 cells (f) in the colonic lamina propria (n = 6). Representative flow cytometry plots for CD4+Foxp3+ Tregs (upper panels) and CD4+IL-17A+ Th17 cells (lower panels) in the colonic lamina propria were shown in (d). All data are presented as mean ± SEM. Statistical significance was assessed by one-way ANOVA with post hoc multiple comparisons. $p < 0.05$, $p < 0.01$, $p < 0.001$. ns, not significant.

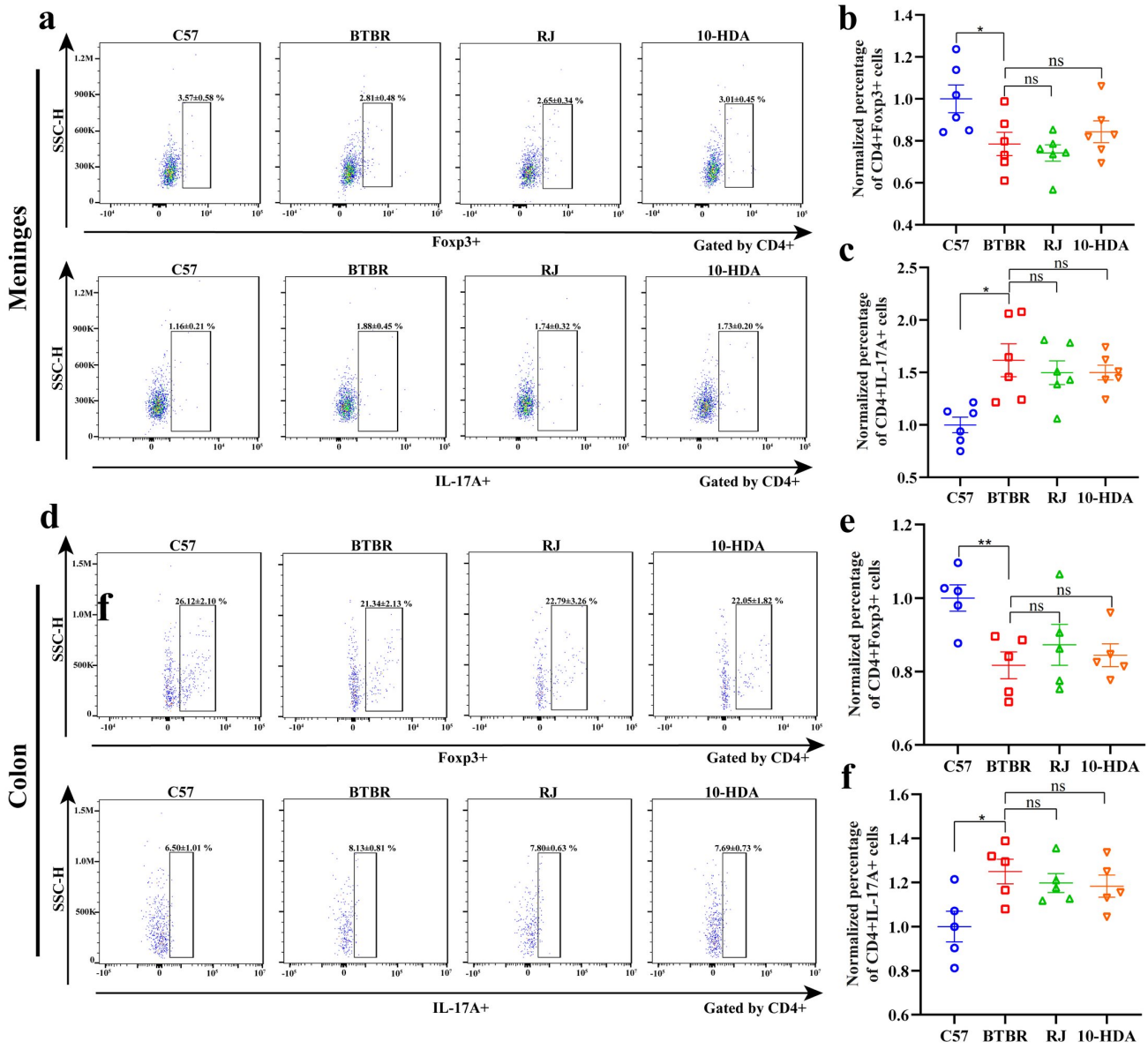


*Supplementary Figure S2*

Supplementary Figure S3. Gut microbiome diversity profiling and supplementary analyses of the FMT experiment. (a) Venn diagram illustrating the overlap of operational taxonomic units (OTUs) among C57BL/6J (C57), BTBR, and BTBR+10-HDA mice, as determined by 16S rRNA sequencing. (b) Principal component analysis (PCA) of 16S rRNA sequencing data, illustrating the separation of gut microbial communities. (c-e) Relative abundance of Firmicutes (c), Bacteroidota (d) and their relative ratio (e) in the gut microbiome. (f) Schematic timeline of the fecal microbiota transplantation (FMT) experiment, in which germ-free or antibiotic-depleted recipient BTBR mice were colonized with fecal microbiota harvested from BTBR or BTBR+10-HDA donors over three week. (g) Quantification of interaction time with Mouse 1 versus Mouse 2 during the social novelty phase of the three-chamber test in BTBR and FMT recipient groups (n = 6). (h) Number of marbles buried in the marble burying test (n = 6). All data are presented as mean ± SEM. Statistical significance was assessed by two-way ANOVA for three-chamber trial, one-way ANOVA with post hoc multiple comparisons for multi-group comparisons, and two-tailed Student's t-test for two-group comparisons. $p < 0.05$, $p < 0.01$, $p < 0.001$. ns, not significant.

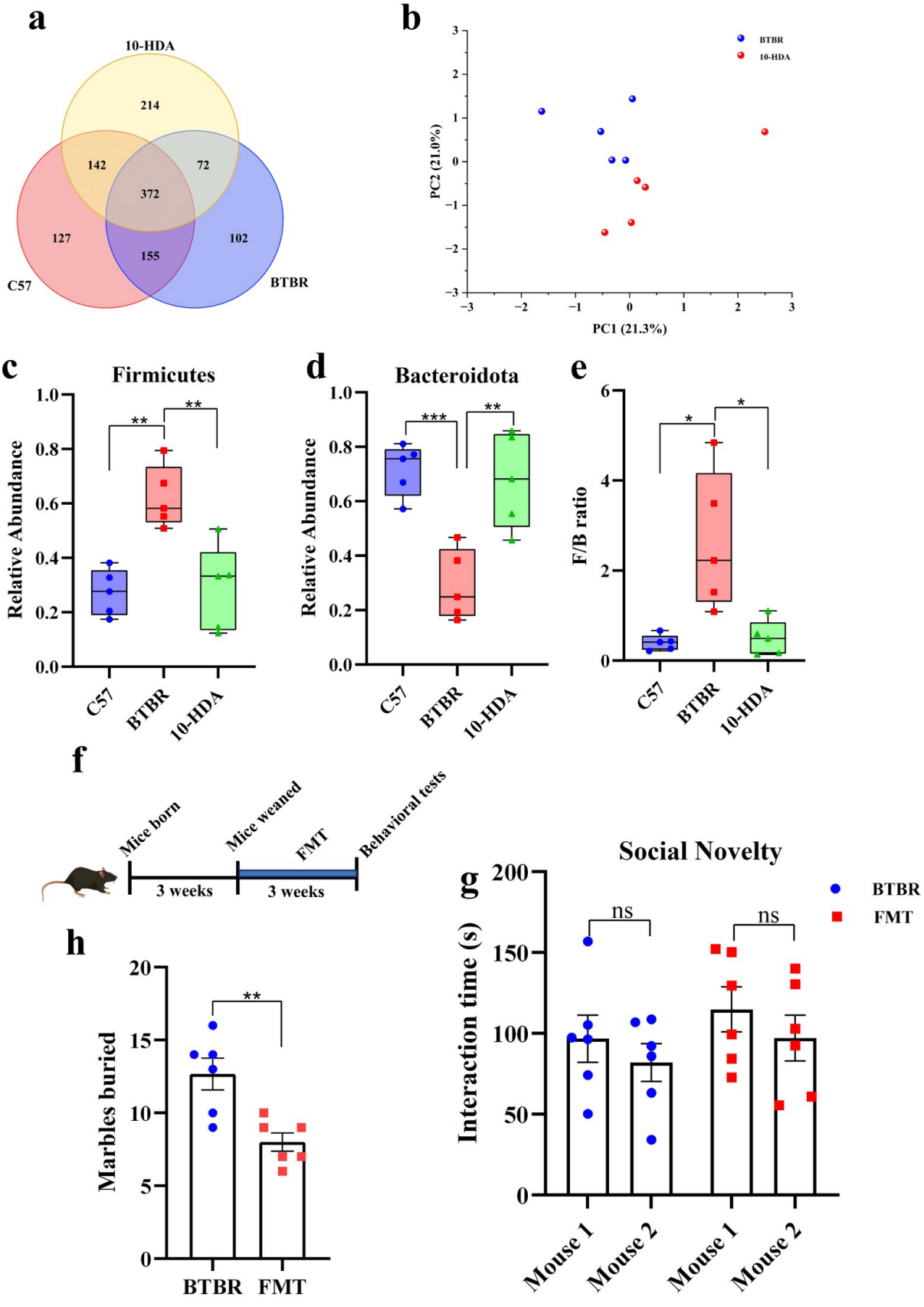


*Supplementary Figure S3*

Supplementary Figure S4. Antibiotic-induced gut dysbiosis disrupts microbial community composition and mPFC transcriptomic homeostasis. (a) Venn diagram illustrating the overlap of OTUs among the antibiotic-treated (ABX), BTBR, and BTBR+10-HDA groups, based on 16S rRNA sequencing. (b) Cladogram depicting the phylogenetic distribution of differentially abundant microbial taxa, as identified by LEfSe analysis. (c) Venn diagram illustrating the overlap of expressed genes in the mPFC of mice treated with both 10-HDA and antibiotics, based on transcriptomic profiling. (d) Volcano plot of differentially expressed genes (DEGs) in the mPFC of BTBR+10-HDA mice relative to BTBR conspecifics, with upregulated and downregulated genes shown in red and green, respectively. The horizontal dashed line indicates $p = 0.05$. (e) Volcano plot of DEGs in the mPFC of BTBR+10-HAD+ABX mice relative to BTBR+10-HDA conspecifics. (f) KEGG pathway enrichment analysis of DEGs identified in vancomycin-treated mice upon microbiome dysbiosis. Bubble size represents gene count and color indicates the significance of difference. (g) Social novelty test in mice involved in microbiome dysbiosis trials ($n = 6$). All data are presented as mean ± SEM. Statistical significance was assessed by two-way ANOVA for the three-chamber trial. $p < 0.05$, $p < 0.01$, $p < 0.001$. ns, not significant.

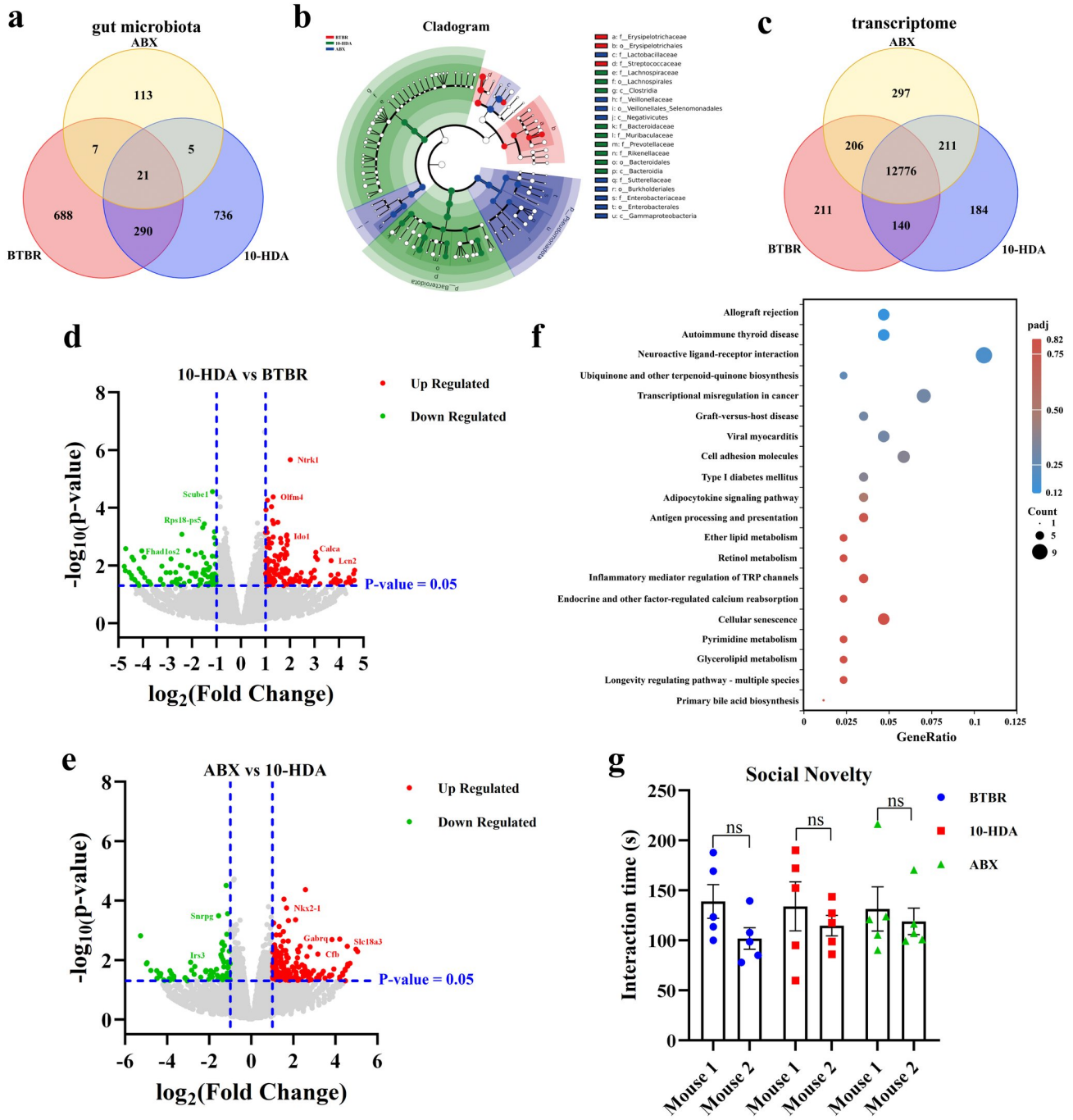


*Supplementary Figure S4*

Supplementary Figure S5. Metagenomic pathway profiling and transcriptomic characterization of mPFC responses to IL-6 blockade. (a) Metagenomic KEGG pathway annotation comparing gene counts between BTBR and BTBR+10-HDA mice across selected metabolic pathways, including propanoate metabolism, as determined by metagenomic sequencing. (b) Venn diagram illustrating the overlap of expressed genes in the mPFC between BTBR and Anti-IL-6-treated mice. (c) Principal component analysis (PCA) of mPFC transcriptomic profiles in BTBR mice with IL-6 blockade. (d) Heatmap depicting the expression levels of representative DEGs with selected genes annotated on the right. (e) Quantification of interaction time with Mouse 1 versus Mouse 2 during the social novelty phase of the three-chamber test in BTBR and Anti-IL-6-treated groups (n = 6). All data are presented as mean ± SEM. Statistical significance was assessed by two-way ANOVA for the three-chamber trial. $p < 0.05$, $p < 0.01$, $p < 0.001$. ns, not significant.

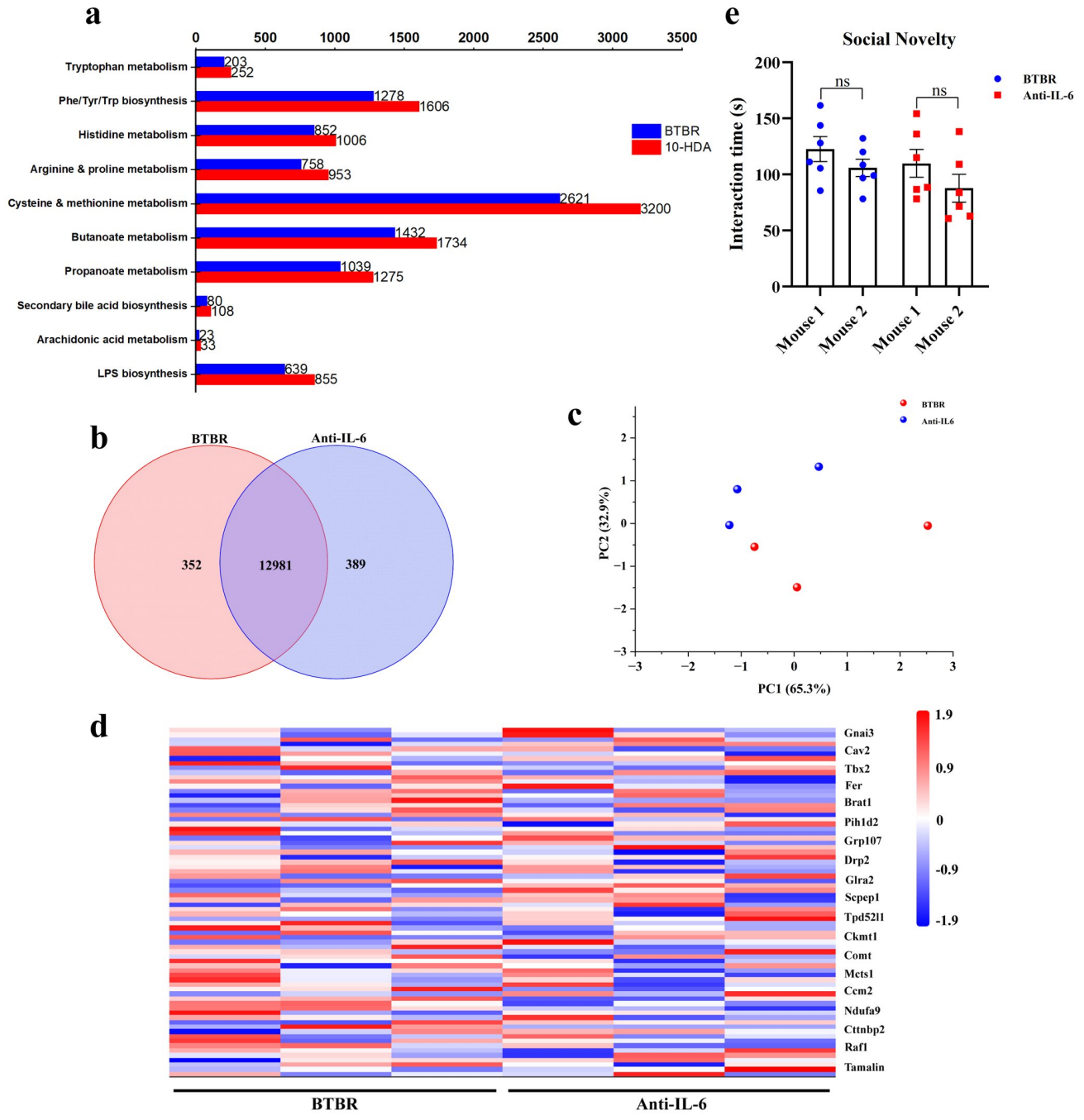


*Supplementary Figure S5*

Supplementary Figure S6. Molecular docking analysis and characterization of 10-HDA-induced histone methylation landscapes. (a) AutoDock Vina docking score (mean ± SD Vina binding affinity across three independent random seeds, 42/123/2026; individual seed values shown as black points) for 10-HDA against the H3K4me3 and H3K27me3 modified H3 tail peptides, using the receptor structures and search parameters described in Methods (Molecular Docking). (b) Number of receptor polar-atom contacts within 3.5 Å of the top-scoring pose (grey bars) alongside the corresponding mean magnitude of Vina affinity (red bars) for each site. (c) Representative Integrative Genomics Viewer (IGV) browser tracks of H3K4me3 and H3K27me3 CUT&Tag read-density signal at the Foxp3 locus in Treg-polarized CD4+ T cells in the presence or absence of 10-HDA. (d) ChIP-qPCR analysis of H3K4me3 and H3K27me3 enrichment at the Foxp3 locus in untreated and 10-HDA-treated Treg-polarized CD4+ T cells, expressed as percentage of input (n = 4). (e) KEGG pathway enrichment analysis of genes exhibiting differential H3K4me3 occupancy upon 10-HDA treatment in Treg-polarized CD4+ T cells. Bubble size represents the number of enriched genes and color gradient indicates q-value. (f-g) GO term enrichment of genes bearing H3K27me3 marks in vehicle-treated (f) and 10-HDA-treated (g) Treg-polarized CD4+ T cells, respectively. All data are presented as mean ± SEM. Statistical significance was assessed by two-tailed Student's t-test. $p < 0.05$, $p < 0.01$, $p < 0.001$. ns, not significant.

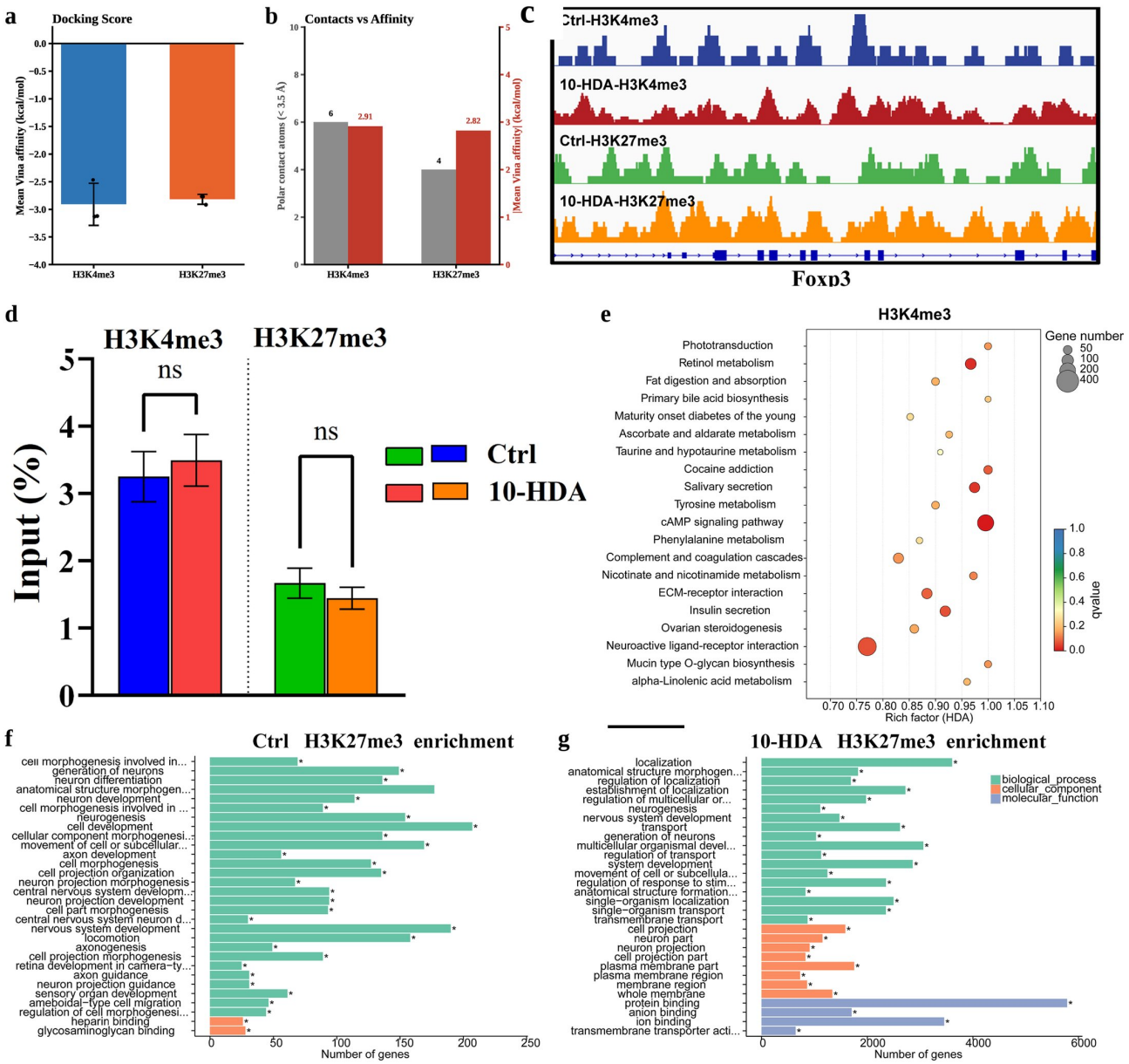


*Supplementary Figure S6*